Multi-Species Hybrid Ion Acceleration from ps, PW interactions with Ultra-Thin Foils.

Contact: omccusker03@qub.ac.uk

O. McCusker, A. McIlvenny, P. Martin, S. Ferguson, S. Zhai, S. Kar, M. Borghesi
Centre of Plasma Physics, Queen's University Belfast, BT7 1NN, UK

J. Jarrett, M. King, P. McKenna
SUPA Department of Physics University of Strathclyde, Glasgow, G4 0NG, UK,

H. Ahmed, J. Green
Central Laser Facility, STFC Rutherford Appleton Laboratory, Oxfordshire OX11 0QX, UK

Abstract

The optimisation of heavy and light ion acceleration from intense laser interactions was investigated experimentally. Ultra-thin (10 - 340 nm) plastic (CH) foils were irradiated with intense, short (750 fs) laser pulses with maximum energies of 75 MeV and 25 MeV/μ obtained for H^+ and C^{6+} ions, respectively. Species resolved spectra suggest differences in the acceleration mechanism for each species. Further analysis through Particle in Cell simulations, identifies a hybrid acceleration scheme, which is enhanced by the onset of relativistically induced transparency. This report presents the analysis of the interplay of the different mechanisms and how it affects each species' acceleration dynamics.

1 Introduction

Laser driven ions have gained significant attention in light of many unique properties such as high brightness, ultrashort emission and low beam emittance[1], offering a range of potential applications in healthcare, industry and nuclear physics [2]. Despite these promising properties, improvements must be made in terms of energy conversion efficiency, spectral beam control and energy selection before these ions can be efficiently employed in several of these applications[3].
The most studied acceleration mechanism is Target Normal Sheath Acceleration (TNSA), which accelerates ions via an electric field generated at the rear target surface and preferentially accelerates lighter ions, such as protons[4]. Amongst alternative mechanisms, Radiation Pressure Acceleration (RPA) is attracting significant interest due to its superior ion energy scaling, although it requires much more stringent conditions in comparison to TNSA. RPA occurs from the momentum transfer from the laser directly to the target and exists in two main modes; hole boring (thick targets)[5] and light sail (thin targets)[6]. RPA is halted by the onset of relativistically induced transparency, however, under suitable conditions, transparency can also enhance acceleration by increasing the magnitude of the accelerating fields[7]. In an experimental setting, isolating the effects of individual acceleration mechanisms is usually a challenging task, as ion acceleration typically results from a combination of different processes [8][9].

2 Experimental Set-up & Results

An experimental campaign was carried out using the petawatt arm of the Vulcan laser. The laser was focused onto target using a $f/3$ off axis parabolic mirror down to a Gaussian spot of 5μm(FWHM) after the use of a plasma mirror. The pulse duration was 750fs(FWHM) containing a total energy of around 210J with around 35% of this in the FWHM of the focal spot, leading to intensities within the range (3-5)$\times 10^{20}$Wcm^{-2}. Plastic (CH) targets of various thicknesses in the range 10nm-340nm were used and aligned so that the surface was normal to the laser axis. The main diagnostics used for measuring the spectra of the accelerated ions were Thomson Parabola Spectrometers (TPS), placed in the forward direction at five different angles: 6.5°, 2.2°, −6.5°, −10.8° and −19.2° with respect to the laser axis. A schematic of the experimental set-up can be seen in Figure (1)

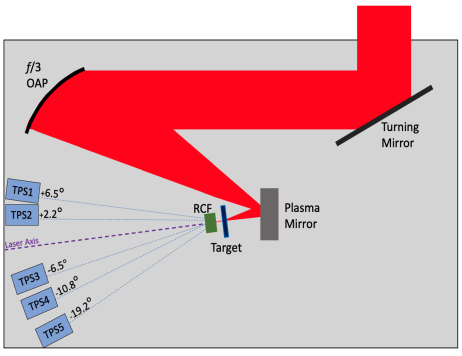

Figure 1: Simplified schematic of the experimental setup.

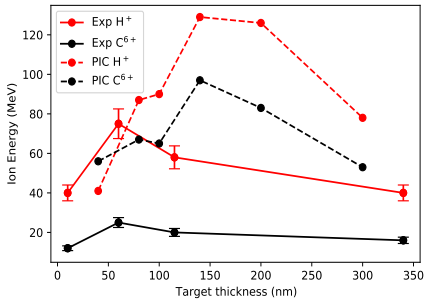

Figure 2: Maximum energies obtained both experimentally and through PIC simulations(dashed lines) for both species, H^+ (red) and C^{6+} ions (black).

An optimal target thickness for acceleration of both protons and carbon ions was obtained from a thickness scan, shown in Figure (2). A similar trend in the maximum energies achieved vs target thickness for each species is seen. Maximum energy for both species is observed at 60nm thickness, i.e. 75MeV for protons and 25MeV/μ for carbon ions. The maximum energies were obtained on TPS1 placed at +6.5°; a comparison of the spectra obtained for three target thicknesses; (10nm, 60nm and 340nm) is shown in Figure (3). All spectra, except that at the optimum thickness, display the exponentially decaying feature which is typical of TNSA accelerated ions. At a foil thickness of 60nm the ion energies are significantly higher, and a peak can be identified at around 60MeV and 23MeV/μ, for protons and carbon ions, respectively (more pronounced for carbon ions). This feature is most likely resulting from an interplay of TNSA and RPA-LS mechanisms, similar to described in ref. [10][11].

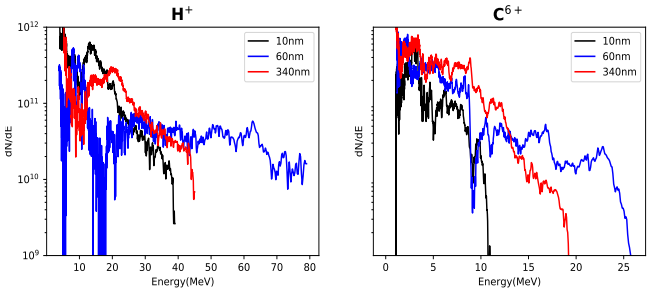

Figure 3: Spectra obtained for both H^+ (left) and C^{6+} (right) ions at TPS1 (+6°) for three target thicknesses, 10nm, 60nm and 340nm.

Moreover, a much flatter profile prior to the high energy peak is observed at 60nm for protons, compared to carbon ions, suggesting differences in the acceleration of the two species, which is further investigated using PIC simulations.

3 2D PIC Simulations

The relativistic PIC code EPOCH [12] was used to carry out 2D simulations. The targets were initialised with an electron density of 600 n_c, where n_c is the critical density (1×10^{21} cm^{-3}) and neutralised with a uniform mixture of C^{6+} and H^+. The target thicknesses were varied from 40nm to 300nm and the size of the simulation box was 80μm by 20μm (x and y) with a mesh cell size equal to 5nm × 10nm. The laser pulse temporal and spatial profiles were both Gaussian with FWHM equal to 0.6ps and 5μm, respectively and the peak intensity was equal to 5 $\times 10^{20}$Wcm^{-2}. The target was located at x=0 and irradiated at normal incidence.
Initially a thickness scan was carried out, seen in Figure (2), showing an optimal thickness of 140nm. The thicker optimal target thickness obtained in the simulations (140nm compared to 60nm) is accounted for by the fact that in the 2D simulations there are reduced degrees of freedom, and so the target's transverse expansion is limited, delaying the onset of relativistic transparency. In a 3D case, this will occur earlier (with respect to the 2D simulations) and shift the optimal conditions to thinner targets since the enhanced acceleration is based on volumetric heating through a relativistically underdense plasma. Despite these differences, the physical processes should however remain the same.

At the optimal target thickness, 140nm, the evolution of the electric (accelerating) field was studied as well as its effect on ion densities. Figure (4) shows the electric fields at three time-steps: before, during and after transparency.

Figure (4)a) and b) highlight a dual peaked electric field and the initial expansion of the ion densities, where R and S represent the RPA and TNSA fields, respectively. As expected the protons have expanded further than the carbon ions, due to the preferential acceleration of protons by TNSA. At this early time, a distinct peak in the proton density is identified travelling slightly behind the TNSA field. This may be due to the space charge of the carbon ions which have been accelerated at this point, piling a bunch of protons locally into a peak. At the point of target transparency, seen in Figure(4)c) and d), an increase in the electric field is seen to around 6TVm^{-1} at the target surface. Comparing ion densities at this time, it is seen that the heavier carbon bulk undergoes a reduced expansion; due to this it will be in a better position to benefit from the transparency enhanced fields as the laser breaks through. This boost in the electric field is maintained after the peak of the pulse arrives on target, as seen in Figure (4)e) and f) with further expansion of both ions. Despite no longer being as pronounced and having partly merged, both R and S fields have also increased in magnitude (∼5TVm^{-1}). However, the highest field strength remains around the target centre (between 0μm and 5μm in x), raising ques-

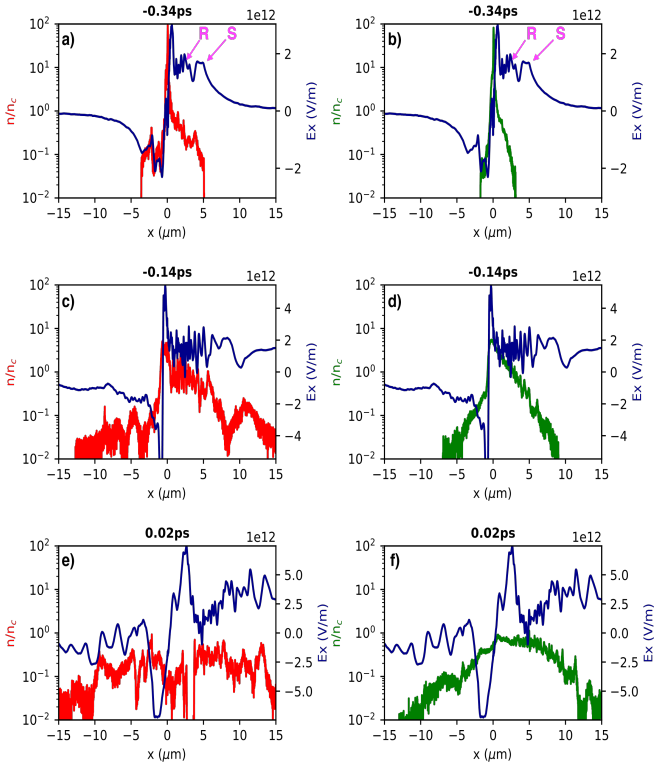

Figure 4: Cycle averaged electric fields (E_x, i.e. along the laser axis) with H^+ (red) and C^{6+} (green) density. (a) and (b) are taken at t =-0.34ps, (c) and (d) are at t= -0.14s (when target goes transparent) and (e) and (f) are at t=0.02ps, where t=0ps corresponds to the peak of the pulse arriving on target.

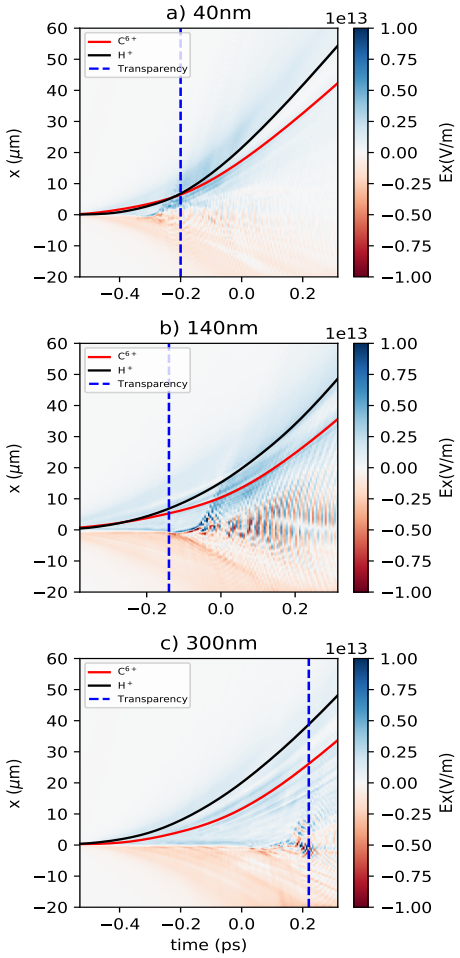

Figure 5: 2d colour-maps of average electric field at each time-step for three thicknesses, a)40nm, b)140nm, c)300nm. X positions of highest energy ions (H^+ (black) and C^6+ ions (red)) for each thickness are tracked. The times at which transparency occurs are marked with a blue vertical line for each thickness.

tions as to which field/fields are responsible for acceleration of the highest energy ions.

To further investigate this, ID tracking was employed within the simulations. Each individual ion is assigned an ID as it is initialised and so their individual movement can be tracked, which allows differences in the acceleration of each species to be identified. In particular, we tracked, for both species, the ions which at the end of the simulation have energies within 5 MeV/nucleon from the maximum energy observed in the spectrum. Additionally, two other thicknesses have also been considered; 40nm and 300nm, for comparison. The cycle-average electric fields along the target normal throughout the interaction have been plotted in Figure (5) in 2d colour-maps, with corresponding average x positions for each ion species at each time also mapped, highlighting the fields which these ions experience throughout their acceleration. The time at which the target goes transparent is also marked on the plot.

For the 40nm target, transparency occurs early in the interaction(-0.22ps), after which an increase in the electric field is seen. The tracked ions follow a maximum strength peak, and a slight increase in their acceleration is seen after transparency. However, this boost in the field is not maintained for very long, with the field which the tracked ions experience decreasing shortly after the arrival of the peak of the pulse. For optimal thickness, 140nm, an increase in the electric field is also seen after transparency (Figure(5)b)), this time reaching a much more significant amplitude, $\sim 10TVm^{-1}$, which is maintained throughout the interaction. In response to these increased fields, acceleration of both protons and carbon ions also increases, with protons (also seen in Figure (4)), at the forefront of the accelerated ion beam. For the thickest foil, 300nm, transparency occurs after the peak of the pulse arriving on target and it plays little role in the acceleration of the tracked ions. An increase in the field is shown after this time, in Figure(5)c), however at this point highest energy ions have been significantly ac-

celerated and have moved away from this position and so the enhanced fields have little effect on them.

To further pinpoint differences between acceleration of protons and carbon ions for 140nm, the electric fields which the tracked ions experience at different times are plotted, for both species, in Figure(6).

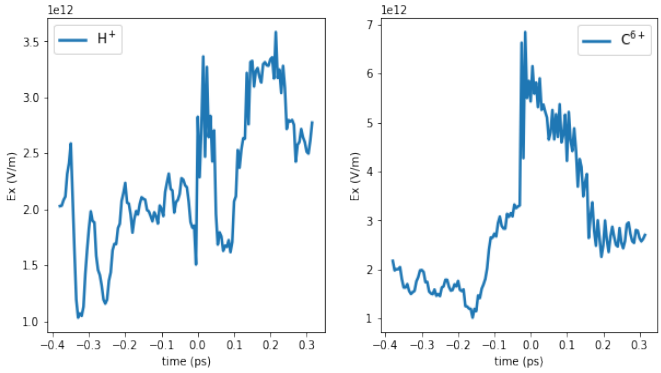

Figure 6: Averaged electric field experienced by maximum H^+ (left) and C^6+ ions (right) throughout the interaction for optimal target thickness, 140nm.

Distinct differences can be seen between the two species, with protons experiencing a maximum field strength of 3.5TVm^{-1} initially at 0μm (as the peak of the laser pulse arrives), then again at 0.2ps. Carbon ions also experience their maximum field at 0ps, however a much greater amplitude of $7\times10^{12}\text{Vm}^{-1}$ is experienced within a single peak. The different peaks within the electric field experienced by the protons may be due to proton bunches ultimately ending up in the top energy range. As seen in Figure(4), there is significant proton acceleration from the front surface of the target early in the interaction, which could account for some of these high energy protons. However, with the significant increase in the electric fields after transparency, protons which have remained within the bulk of the target and experience this strong field could also be accelerated over a shorter time to maximum energy. The suggestion that multiple proton bunches eventually end up with maximum energy could potentially explain not only the numerous peaks seen in the electric field in Figure(6) (as an average field experienced by these protons was considered), but also why a flatter proton spectrum was obtained experimentally for 60nm.

The highest energy carbon ions experience a much greater field after 0ps, suggesting that these ions remained within the target bulk until this time and were picked up by this very large field and accelerated. Also the single distinct peak seen in this electric field would suggest that one single bunch of ions which experience the same accelerating fields reach maximum energy. Further analysis is being conducted to confirm these interpretations.

4 Conclusions

In summary, observations of thickness-dependent proton and carbon ion spectra from ultra-thin foils are interpreted with the help of 2D PIC simulations. PIC simulations corroborate experimental results and elucidate a complex interplay of different mechanisms with differing effect on light and heavy ion species. For instance, protons are observed to originate from both the front surface of the target and bulk of the target. Simulations suggest the proton acceleration is enhanced by relativistic transparency, where generation of various accelerating fields within the duration of pulse leads to acceleration of protons in a broad energy spread. On the other hand, highest energy carbon ions appear to originate from within the target bulk and are accelerated by transparency-enhanced fields continuously over an extended length. Further analysis will be dedicated to better deconvolve the multi-species dynamics observed in the interaction.

References

[1] A. Macchi, M. Borghesi, and M. Passoni. Ion acceleration by superintense laser-plasma interaction. *Rev. Mod. Phys.*, 85:751–793, May 2013.

[2] Matteo Passoni, Francesca Arioli, Lorenzo Cialfi, David Dellasega, Luca Fedeli, Arianna Formenti, Anna Chiara Giovannelli, Alessandro Maffini, Francesco Mirani, Andrea Pazzaglia, Alessandro Tentori, Davide Vavassori, Margherita Zavelani-Rossi, and Valeria Russo. Advanced laser-driven ion sources and their applications in materials and nuclear science. *Plasma Physics and Controlled Fusion*, 62, 11 2019.

[3] J Badziak. Laser-driven ion acceleration: methods, challenges and prospects. *Journal of Physics: Conference Series*, 959:012001, jan 2018.

[4] S. C. Wilks, W. L. Kruer, M. Tabak, and A. B. Langdon. Absorption of ultra-intense laser pulses. *Phys. Rev. Lett.*, 69:1383–1386, Aug 1992.

[5] Andrea Macchi, Tatyana Liseykina, Sara Tuveri, and Silvia Veghini. Theory and simulation of ion acceleration with circularly polarized laser pulses. *Comptes Rendus Physique, v.10, 207-215 (2009)*, 10, 03 2009.

[6] Andrea Macchi, Silvia Veghini, and Francesco Pegoraro. "light sail" acceleration reexamined. *Phys. Rev. Lett.*, 103:085003, Aug 2009.

[7] F. Cattani, A. Kim, D. Anderson, and M. Lisak. Threshold of induced transparency in the relativistic interaction of an electromagnetic wave with overdense plasmas. *Phys. Rev. E*, 62:1234–1237, Jul 2000.

[8] A. Higginson, R. J. Gray, M. King, R. J. Dance, S. D. R. Williamson, N. M. H. Butler, R. Wilson, R. Capdessus, C. Armstrong, J. S. Green, S. J. Hawkes, P. Martin, W. Q. Wei, S. R. Mirfayzi, X. H. Yuan, S. Kar, M. Borghesi, R. J. Clarke, D. Neely, and P. McKenna. Near-100 mev protons via a laser-driven transparency-enhanced hybrid acceleration scheme. *Nature Communications*, 9, 2 2018.

[9] H. Padda, M. King, R. J. Gray, H. W. Powell, Bruno Izquierdo, L. C. Stockhausen, R. Wilson, D. C. Carroll, R. J. Dance, D. A. MacLellan, X. H. Yuan, N. M. H. Butler, R. Capdessus, M. Borghesi, D. Neely, and P. McKenna. Intra-pulse transition between ion acceleration mechanisms in intense laser-foil interactions. *Physics of Plasmas*, 23(6), June 2016.

[10] K. F. Kakolee, M. Borghesi, M. Zepf, S. Kar, D. Doria, B. Ramakrishna, K. Quinn, G. Sarri, J. Osterholz, M. Cerchez, O. Willi, X. Yuan, and P. McKenna. Scaling of ion spectral peaks in the hybrid rpa-tnsa region. *Journal Of The Korean Physical Society*, 68(6):768–771, 3 2016.

[11] Bin Qiao, Satyabrata Kar, Michael Geissler, P. Gibbon, Matthew Zepf, and Marco Borghesi. Dominance of radiation pressure in ion acceleration with linearly polarized pulses at intensities of 10(21) w cm(-2). *Physical Review Letters*, 108(11), 3 2012.

[12] T Arber, Keith Bennett, C Brady, A Lawrence-Douglas, M Ramsay, N Sircombe, P Gillies, R Evans, Holger Schmitz, A Bell, and Cp Ridgers. Contemporary particle-in-cell approach to laser-plasma modelling. *Plasma Physics and Controlled Fusion*, 57, 11 2015.